

# An Examination of Polarization Mode Transitions in Pulsar Radio Emission

M. M. MCKINNON<sup>1</sup>

<sup>1</sup>*National Radio Astronomy Observatory, Socorro, NM 87801 USA*

## ABSTRACT

A statistical model is used to determine how stochastic fluctuations in the intensities of orthogonal polarization modes contribute to the modulation and depolarization of pulsar radio emission. General expressions for the distributions of the Stokes parameters, linear polarization, polarization position angle, and fractional polarization are derived when the mode intensities follow the same or different probability distributions. The transition between modes is examined. When the mode intensities follow the same distribution, the fractional linear polarization and modulation index are symmetric about the transition. The symmetry is disrupted when the mode intensities follow different distributions. The fractional linear polarization is minimum and the mode frequency of occurrence changes rapidly at transitions where the mode intensity distributions are the same and the modulation index is small. A lower limit on the fractional linear polarization that can be attained via the simultaneous occurrence of the modes as a function of modulation index is quantified.

## 1. INTRODUCTION

The radio emission from pulsars is highly linearly polarized. The position angle (PA) of the emission's polarization vector observed in individual pulses and average profiles frequently changes discontinuously by  $\pi/2$  radians, suggesting the emission is comprised of two modes of orthogonal polarization (OPMs; Manchester, Taylor, & Huguenin 1975). The OPMs appear to be a common, if not ubiquitous, feature of the emission (Manchester, Taylor, & Huguenin 1975; Backer & Rankin 1980; Stinebring et al. 1984). The depolarization of the emission with increasing radio frequency (Manchester, Taylor, & Huguenin 1973; Morris, Graham, & Sieber 1981) has been attributed to OPMs occurring with comparable frequency and similar strength (e.g. Stinebring et al. 1984; McKinnon 1997, 2004; Karastergiou et al. 2002; Smits et al. 2006).

The radio emission is also heavily modulated. The modulation index of the total intensity, the ratio of its standard deviation to its mean,  $\beta$ , can vary over  $0.1 < \beta < 2$  across a pulsar's pulse and across the pulsar population (e.g. Bartel, Sieber, & Wolszczan 1980; Weisberg et al. 1986; Weltevredre et al. 2006, 2007; Burke-Spolaor et al. 2012). The modulation is often attributed to subpulse drift, where subpulses move across the overall pulse envelope in an organized pattern (e.g. Taylor, Manchester, & Huguenin 1975; Deshpande & Rankin 2001). In those instances where the observer's sight line tangentially traverses the pulsar's radio beam, the modulation index resulting from subpulse drift

can be relatively low and constant across the pulse, where the subpulses can occur regularly from pulse to pulse, and increases toward the pulse edges, where the subpulses appear to enter and exit the pulse envelope (Rankin 1986; Weisberg et al. 1986). The drift pattern is consistent with a carousel of emission sparks circulating about the pulsar polar cap that is ascribed to  $\mathbf{E} \times \mathbf{B}$  drift (Ruderman & Sutherland 1975; Gil & Sendyk 2000).

The modulation and OPMs likely conspire to depolarize the emission. With details depending upon the polarization of the individual subpulses, the occurrence of OPMs within them, and the subpulse drift pattern, the aggregate linear polarization will decrease as subpulses within consecutive pulses of the star are summed to create the pulsar’s average profile. Rankin & Ramachandran (2003) proposed that the polarization of PSR B0809+74, an exemplar of drifting pulsars, was determined by two circulating systems of subpulses, with one system dominated by one polarization mode and the other system dominated by the other mode. Their model required the circulating systems to be out of phase, with one of the systems shifted further away from the magnetic axis than the other. A detailed analysis of the pulsar’s polarization by Edwards (2004) confirmed their interpretation, but only at 328 MHz. He also found the complex polarization properties of two other drifting pulsars, PSR B0320+29 and PSR B0818-13, were difficult to reconcile with the Rankin & Ramachandran model. Clemens & Rosen (2004, 2008) developed a self-consistent model of subpulse drift and OPMs that attributes the drift to nonradial oscillations of the neutron star or its magnetosphere. In their model, coherent emission from one of the OPMs, the “displacement polarization mode”, is modulated by pulsational displacements. The emission from the other OPM, the “velocity polarization mode”, is modulated by pulsational velocities. Their model produces a reasonable facsimile of the drifting subpulses and polarization in PSR B0940+10 (Rosen & Clemens 2008) and PSR B0809+74 (Rosen & Demorest 2011). An important clarification to be made here is the modulation and depolarization of the emission by subpulse drift, regardless of its origin, is a *systematic* process.

Not all pulsars, however, exhibit subpulse drift (Weltevrede et al. 2006, 2007), and the switching between OPMs is generally regarded as a *stochastic* process (Cordes, Rankin, & Backer 1978). The emission has been accurately modeled as a stochastic sequence of polarization states with structure having several characteristic timescales (Cordes 1976a, 1976b; Cordes & Hankins 1977). Additionally, while some assessments of subpulse drift assume the radiation from a subpulse is steady and unmodulated (e.g. Jenet & Gil 2003), the observed subpulse structure is variable and complex and cannot be attributed to instrumental noise (see, e.g., Figures 2-5 in Gil & Sendyk (2000) for PSRs B0943+10, B2303+30, B2319+60, and B0031-07; Figure 1 of Cordes (1976a) for PSR B2016+28; and the discussion of a stochastic component in the emission of PSR B0943+10 in Rosen & Clemens (2008)). Therefore, while the process that modulates and depolarizes the emission from some pulsars may be systematic, it may be stochastic, or both, in others.

A statistical model for the polarization of pulsar radio emission established a connection between OPMs and intensity modulation (McKinnon & Stinebring 1998, hereafter MS). The model assumes the emission is comprised of two independent, simultaneously occurring, completely polarized orthogonal modes. The model treats the mode intensities as random variables (RVs) to account for the emission’s variability, and consequently focuses on stochastic fluctuations of the emission. The details of the model, its theoretical underpinnings, and the recipe for its implementation can be found in MS and McKinnon (2022; hereafter M22). Since the modes are orthogonal, their polarization vectors are antiparallel in the Poincaré sphere; therefore, the model predicts that polarization fluctuations

occur along a diagonal in the sphere. One might reasonably conclude that polarization fluctuations are large when the total intensity is heavily modulated, but absent the model, it is not intuitively obvious that the polarization fluctuations have a preferred orientation in the sphere, as the model requires. When multiple samples of the Stokes parameters  $Q$ ,  $U$ , and  $V$  recorded at a specific pulse phase are plotted in the Poincaré sphere, the shape of the resulting cluster of data points is a prolate ellipsoid. Absent any other emission component, the size of the ellipsoid’s major axis is determined by a combination of the polarization fluctuations and instrumental noise, while the sizes of the ellipsoid’s minor axes are set by the instrumental noise alone (McKinnon 2004, hereafter M04). The axial ratio of the major axis is approximately  $(1 + s^2\beta^2)^{1/2}$ , where  $s$  is the signal-to-noise ratio of the total intensity (M04) and  $\beta$  is its modulation index. The axial ratio is large where the signal-to-noise ratio and modulation index are also large. This prediction was found to be generally true for PSR B2020+28 and PSR B1929+10 (M04) and in the outriders of PSR B0329+54 (Edwards & Stappers 2004, hereafter ES04). The model and observations suggest randomly fluctuating OPMs play a role in determining both the observed polarization and modulation of the emission.

The MS statistical model can be used to derive distributions of the Stokes parameters of the combined radiation, its linear polarization, fractional polarization, and PA given the distributions of the individual mode intensities. In the implementation of the model in MS and M22, the statistical character of the mode intensities was assumed to be the same. The mode intensities were assumed to be Gaussian RVs with identical standard deviations in MS. The distributions produced by the model were varied by altering the mean intensity of one mode relative to that of the other. In M22, the mode intensities were assumed to be exponential RVs to account for the heavy modulation of the total intensity, the correlation of the Stokes parameters, and observed asymmetries in distributions of total intensity, polarization, and fractional polarization. The primary conclusion from M22 was the mode intensities must have different variances to explain what is observed. The difference in variances was attributed to either different emission mechanisms for the modes or to mode-dependent propagation or scattering effects in the pulsar magnetosphere. Summarizing, previous implementations of the model explored the effects of varying the means (MS) and variances (M22) of mode intensities that followed the same distribution. The next logical step in this line of investigation is to explore how mode intensities of different statistical character might affect what is observed, as there appears to be no a priori reason for them to follow the same distribution.

The primary objectives of this paper are twofold. The first is to explore the polarization and modulation properties of the emission when the mode intensities follow different probability distributions. The second is to conduct a detailed examination of a transition between modes in an average pulse profile. The analysis assumes the functional form of a mode’s intensity distribution is retained throughout the short duration of a transition, but the relative scaling of the two distributions varies across it. The variation in the relative scaling of the two distributions drives the transition between the modes and causes the modulation index to vary across the transition.

The paper is organized as follows. The model is implemented in Section 2 assuming the mode intensities follow different Erlang distributions. The Erlang distribution was chosen for the analysis because it can produce a range of modulation indices that approaches what is observed in pulsar radio emission, and it allows analytical solutions within the context of the statistical model. The assumption of Erlang mode intensities also enables a general implementation of the MS statistical model of which the Gaussian and exponential intensities considered in MS and M22 are specific

cases. Distributions of the emission's Stokes parameters, linear polarization, fractional polarization, and polarization position angle at a given pulse phase are derived. Statistical parameters that characterize the emission and its polarization are also derived. The salient features of the analysis are highlighted in Section 3. A detailed examination is made of a mode transition, and the effectiveness of randomly fluctuating OPMs in depolarizing the emission is evaluated. The statistical parameters and distributions of fractional polarization derived from Erlang distributions are compared with their counterparts derived from Gaussian distributions. The results of the analysis are discussed and compared with observations in Section 4. Conclusions are summarized in Section 5.

## 2. MODEL IMPLEMENTATION

### 2.1. Review of the Erlang Distribution

The Erlang distribution arises from the sum of  $n$  independent, identically distributed, exponential RVs (e.g. Ross 1984, p. 171), and is given by

$$f(x, \mu, n) = \frac{x^{n-1}}{\Gamma(n)\mu^n} \exp\left(-\frac{x}{\mu}\right), \quad x \geq 0, \quad (1)$$

where  $\mu$  is a positive scaling factor,  $n$  is a positive integer representing the order of the distribution, and  $\Gamma(n) = (n-1)!$  is the gamma function. The Erlang distribution is the exponential distribution when  $n = 1$ . From the central limit theorem, the distribution approaches the Gaussian distribution when  $n$  becomes very large. The  $k^{\text{th}}$  moment of the distribution is

$$\langle x^k \rangle = \frac{\Gamma(n+k)}{\Gamma(n)} \mu^k. \quad (2)$$

The mean of the distribution is  $n\mu$ , and its variance is  $\sigma^2 = n\mu^2$ . The modulation index of the Erlang distribution is  $\beta = 1/\sqrt{n}$ , which is independent of  $\mu$  and decreases with increasing  $n$ .

Since the distribution of the sum of independent RVs is the convolution of their individual distributions (e.g. Papoulis 1965, p. 189), the distribution of the sum of two Erlang RVs having orders  $n_a$  and  $n_b$  and identical scaling factors,  $\mu$ , is also an Erlang distribution with a scaling factor  $\mu$  and order  $n = n_a + n_b$ .

$$f(x, \mu, n_a) * f(x, \mu, n_b) = f(x, \mu, n_a + n_b) \quad (3)$$

### 2.2. Definitions and Nomenclature

The implementation of the statistical model in MS and M22 focused on one of the orthogonal modes remaining the primary (dominant) mode. To be specific, the primary mode as discussed in this paper is defined as the polarization mode that occurs most frequently, as in a PA histogram. By not exploring the possibility of the other mode becoming the primary, MS and M22 did not exploit the full capability of the model. To do so requires minor revisions to the definitions and nomenclature used in the analysis. These revisions do not alter the results or conclusions described in MS and M22. Here, the modes are designated as A and B, without the presumption that one is the primary or secondary mode. When the OPMs are completely linearly polarized, the instantaneous total intensity is the sum of the RVs representing the mode intensities,  $I = X_A + X_B$ , and the Stokes parameter Q is their difference,  $Q = X_A - X_B$  (MS). The remaining Stokes parameters, U and V, are

temporarily assumed to be fixed at zero to simplify the analysis. So defined, the Stokes parameters I and Q will generally, but not always, be correlated when mode A is the primary mode, and will be anticorrelated when mode B is the primary (see Sections 2.4 and 3.1). The scaling factor and order of the mode A Erlang distribution are designated as  $a$  and  $n_a$ , respectively. Similarly, the scaling factor and order of mode B are  $b$  and  $n_b$ .

MS and M22 defined a parameter  $M$  as the ratio of the mode mean intensities,  $M = \langle X_A \rangle / \langle X_B \rangle$ , where the angular brackets denote an average over pulse number at a given pulse phase. That definition is retained in this analysis. The range of  $M$  in MS and M22 was restricted to  $1 \leq M \leq \infty$ , because only one of the modes was viewed as the primary in those analyses. Here, the range of  $M$  is revised to  $0 \leq M \leq \infty$  to accommodate the possibility that either mode can be the primary. M22 also defined a parameter  $m$  as the ratio of the mean Stokes parameter Q to the mean total intensity.

$$m = \frac{\mu_Q}{\mu_I} = \frac{\langle X_A \rangle - \langle X_B \rangle}{\langle X_A \rangle + \langle X_B \rangle} = \frac{M - 1}{M + 1} \quad (4)$$

Its range must be revised from  $0 \leq m \leq 1$  in M22 to  $-1 \leq m \leq 1$ . The emission is comprised solely of mode A when  $m = 1$  ( $M = \infty$ ), and is comprised solely of mode B when  $m = -1$  ( $M = 0$ ). The equations derived in the analysis are simplified when a parameter  $C$  is defined as the ratio of the distribution scaling factors,  $C = a/b$ , along with its complementary parameter  $c = (C - 1)/(C + 1)$ . When  $n_a = n_b$ ,  $M = C$  and  $m = c$ .

Instrumental noise is not included in this particular implementation of the model. The effects of instrumental noise and its treatment in the analysis are discussed in MS, McKinnon (2002), M04, and M22.

### 2.3. Distributions of the Stokes Parameters, Linear Polarization, and Fractional Polarization

The MS statistical model assumes the mode intensities are statistically independent. Therefore, the distribution of the total intensity,  $f_I$ , at a given pulse phase is the convolution of the mode intensity distributions. The distribution resulting from the convolution of two Erlang distributions was derived by Kadri & Smaili (2015). Their Equation 17 rewritten with the nomenclature used in this paper is

$$\begin{aligned} f_I(y, n_a, n_b) &= \int_0^y f(y-x, a, n_a) f(x, b, n_b) dx \\ &= (-1)^{n_a} \left(\frac{b}{a-b}\right)^{n_a} \left(\frac{a}{a-b}\right)^{n_b} \left[ \sum_{k=1}^{n_a} \binom{n_a + n_b - k - 1}{n_b - 1} \left(\frac{b-a}{b}\right)^k f(y, a, k) \right. \\ &\quad \left. + \sum_{k=1}^{n_b} \binom{n_a + n_b - k - 1}{n_a - 1} \left(\frac{a-b}{a}\right)^k f(y, b, k) \right], \quad y \geq 0, \end{aligned} \quad (5)$$

where the leading parenthetical term in each summation is the binomial coefficient. Equation 5 shows that  $f_I$  is an additive combination of weighted Erlang distributions, with the orders of the distributions ranging from  $n = 1$  to the larger of  $n_a$  or  $n_b$ . The equation is valid as long as  $a \neq b$ . When  $a = b$ ,  $f_I$  is a single Erlang distribution with  $n = n_a + n_b$ , as stipulated by Equation 3.

The distribution of the Stokes parameter Q,  $f_Q$ , is the correlation of the mode intensity distributions (MS). The distribution can be derived by replacing the term  $(y+x)^n$  in the correlation with the binomial expansion.

$$\begin{aligned}
f_Q(y, n_a, n_b) &= \int_{-\infty}^{\infty} f(y+x, a, n_a) f(x, b, n_b) dx \\
&= \left(\frac{b}{a+b}\right)^{n_a-1} \left(\frac{a}{a+b}\right)^{n_b} \sum_{k=0}^{n_a-1} \binom{n_a+n_b-k-2}{n_b-1} \left(\frac{a+b}{b}\right)^k f(y, a, k+1), \quad y \geq 0, \\
&\quad \left(\frac{a}{a+b}\right)^{n_b-1} \left(\frac{b}{a+b}\right)^{n_a} \sum_{k=0}^{n_b-1} \binom{n_a+n_b-k-2}{n_a-1} \left(\frac{a+b}{a}\right)^k f(|y|, b, k+1), \quad y < 0 \quad (6)
\end{aligned}$$

Equation 6 shows that  $f_Q$  is also an additive combination of weighted Erlang distributions.

As noted in Section 2.2, the MS statistical model also assumes the Stokes parameter  $U$  is equal to zero, so that the linear polarization is equal to the absolute value of the Stokes parameter  $Q$ ,  $L = (Q^2 + U^2)^{1/2} = |Q|$ . The distribution of linear polarization,  $f_L$ , is the distribution of Stokes  $Q$  folded about  $y = 0$ . Therefore, it is the sum of the two terms in Equation 6 for positive values of  $y$ .

$$\begin{aligned}
f_L(y, n_a, n_b) &= \left(\frac{b}{a+b}\right)^{n_a-1} \left(\frac{a}{a+b}\right)^{n_b} \sum_{k=0}^{n_a-1} \binom{n_a+n_b-k-2}{n_b-1} \left(\frac{a+b}{b}\right)^k f(y, a, k+1) \\
&\quad + \left(\frac{a}{a+b}\right)^{n_b-1} \left(\frac{b}{a+b}\right)^{n_a} \sum_{k=0}^{n_b-1} \binom{n_a+n_b-k-2}{n_a-1} \left(\frac{a+b}{a}\right)^k f(y, b, k+1), \quad y \geq 0 \quad (7)
\end{aligned}$$

When the orthogonal modes are elliptically polarized, the instantaneous values of the Stokes parameters  $Q$ ,  $U$ , and  $V$  at a given pulse phase are simply scaled versions of  $X_A - X_B$  (M22)

$$Q = \cos(2\psi_o) \cos(2\chi_o)(X_A - X_B) \quad (8)$$

$$U = \sin(2\psi_o) \cos(2\chi_o)(X_A - X_B) \quad (9)$$

$$V = \sin(2\chi_o)(X_A - X_B), \quad (10)$$

where  $\psi_o$  is the PA of the mode A polarization vector and  $\chi_o$  is its ellipticity angle<sup>1</sup> (EA;  $\chi_o = 0$  when the modes are linearly polarized, and  $\chi_o = \pm\pi/4$  when the modes are circularly polarized). The distributions of  $Q$ ,  $U$ , and  $V$  are then scaled versions of  $f_Q$  given by Equation 6. The Stokes parameter  $I$  remains the sum of  $X_A$  and  $X_B$ . Consequently, the distributions of all four Stokes parameters and the linear polarization are additive combinations of weighted Erlang distributions.

The procedure for deriving the distributions of fractional polarization is outlined in M22. Without loss of generality, the PA can be set to zero to simplify the analysis. The distribution of fractional circular polarization,  $f_{mv}$ , is derived from the joint probability density of the Stokes parameters  $I$  and  $V$ . The distribution of the fractional linear polarization,  $f_{ml}$ , is derived from the joint probability density of the Stokes parameters  $I$  and  $Q$ . The distributions follow the general forms of

<sup>1</sup> In M22, the colatitude,  $\theta$ , of the mode A polarization vector in the Poincaré sphere was used to represent the polarization's ellipticity. The conventional ellipticity angle,  $\chi$ , is used to represent ellipticity in this analysis.

$$f_{\text{mv}}(z, c, n_a, n_b, \chi_o) = K(c, n_a, n_b) \sin(2\chi_o) \left[ \frac{(\sin(2\chi_o) + z)^{n_a-1} (\sin(2\chi_o) - z)^{n_b-1}}{(\sin(2\chi_o) - cz)^{n_a+n_b}} \right], \quad (11)$$

$$f_{\text{ml}}(z, c, n_a, n_b, \chi_o) = K(c, n_a, n_b) \cos(2\chi_o) \left[ \frac{(\cos(2\chi_o) + z)^{n_a-1} (\cos(2\chi_o) - z)^{n_b-1}}{(\cos(2\chi_o) - cz)^{n_a+n_b}} \right. \\ \left. + \frac{(\cos(2\chi_o) + z)^{n_b-1} (\cos(2\chi_o) - z)^{n_a-1}}{(\cos(2\chi_o) + cz)^{n_a+n_b}} \right], \quad (12)$$

where  $K(c, n_a, n_b)$  is a normalization constant, given by

$$K(c, n_a, n_b) = 2 \left( \frac{1-c}{2} \right)^{n_a} \left( \frac{1+c}{2} \right)^{n_b} \frac{(n_a + n_b - 1)!}{(n_a - 1)! (n_b - 1)!}. \quad (13)$$

The distributions of fractional polarization are functions of four free parameters:  $c$ ,  $n_a$ ,  $n_b$ , and  $\chi_o$ . The range of the independent variable in  $f_{\text{mv}}$  is  $-\sin(2\chi_o) \leq z \leq \sin(2\chi_o)$ , and the range of the independent variable in  $f_{\text{ml}}$  is  $0 \leq z \leq \cos(2\chi_o)$  (M22). When the orders of the mode intensity distributions are the same ( $n_a = n_b = n$ ),  $m = c$ , and the fractional polarization distributions are

$$f_{\text{mv}}(z, m, n, n, \pi/4) = \frac{(1-m^2)^n (2n-1)! (1-z^2)^{n-1}}{2^{2n-1} (n-1)!^2 (1-mz)^{2n}}, \quad (14)$$

$$f_{\text{ml}}(z, m, n, n, 0) = \frac{(1-m^2)^n (2n-1)!}{2^{2n-1} (n-1)!^2} \left[ \frac{(1+mz)^{2n} + (1-mz)^{2n}}{(1-m^2z^2)^{2n}} \right] (1-z^2)^{n-1}. \quad (15)$$

#### 2.4. Model Statistical Parameters

Parameters can be derived to quantify the statistical properties of the emission and its polarization (M22). For OPMs that are completely linearly polarized, the parameters include the mean of Stokes Q relative to the mean total intensity, the modulation index of the total intensity, the correlation coefficient of the Stokes parameters I and Q, the frequency of occurrence of each mode, and the mean fractional linear polarization. The mean of the Stokes parameter Q,  $\mu_Q$ , normalized by the mean total intensity,  $\mu_I$ , is

$$\bar{Q}(c, n_a, n_b) = m = \frac{\mu_Q}{\mu_I} = \frac{n_a(1+c) - n_b(1-c)}{n_a(1+c) + n_b(1-c)}. \quad (16)$$

The normalized Stokes parameter Q is always equal to the parameter  $m$ . It ranges from  $\bar{Q} = 1$  at  $c = 1$  to  $\bar{Q} = -1$  at  $c = -1$ . The transition between modes occurs at  $\bar{Q} = 0$  where the mode mean intensities are equal.

The modulation index of the total intensity is its standard deviation relative to its mean.

$$\beta(c, n_a, n_b) = \frac{\sigma_I}{\mu_I} = \frac{[n_a(1+c)^2 + n_b(1-c)^2]^{1/2}}{n_a(1+c) + n_b(1-c)} \quad (17)$$

The modulation index ranges from that of mode A ( $\beta = 1/\sqrt{n_a}$ ) at  $c = 1$  to that of mode B ( $\beta = 1/\sqrt{n_b}$ ) at  $c = -1$ . The minimum value of  $\beta$  always occurs at  $c = 0$  (i.e. when  $a = b$ ), where

it is given by  $\beta = 1/\sqrt{n_a + n_b}$ . The distribution of the total intensity at  $c = 0$  is a single Erlang distribution (see Equation 3).

The Stokes parameters I and Q are generally covariant. The I-Q correlation coefficient is

$$r_{IQ}(c, n_a, n_b) = \frac{\sigma_a^2 - \sigma_b^2}{\sigma_a^2 + \sigma_b^2} = \frac{n_a(1+c)^2 - n_b(1-c)^2}{n_a(1+c)^2 + n_b(1-c)^2}. \quad (18)$$

The correlation coefficient ranges from  $r_{IQ} = 1$  at  $c = 1$  to  $r_{IQ} = -1$  at  $c = -1$ . It is equal to zero when the variances of the mode intensities are equal.

When  $n_a = n_b = n$ , the parameter  $m$  is equal to  $c$ , and  $r_{IQ}$  and  $\beta$  are given by

$$r_{IQ}(m) = \frac{2m}{1+m^2}, \quad (19)$$

$$\beta(m, n) = \left( \frac{1+m^2}{2n} \right)^{1/2}. \quad (20)$$

The correlation coefficient and normalized mean of Stokes Q are independent of  $n$ . The modulation index remains a function of  $n$ , and varies by a factor of  $\sqrt{2}$  over the full range of  $m$  for a given value of  $n$ .

The distribution of polarization position angle consists of two delta functions separated by  $\pi/2$  radians. The amplitude of the delta function associated with mode A, or the frequency of occurrence of mode A, is the probability that the Stokes parameter Q exceeds zero (MS).

$$\begin{aligned} \nu_a(c, n_a, n_b) &= \int_0^\infty f_Q(y, n_a, n_b) dy \\ &= \left( \frac{1-c}{2} \right)^{n_a-1} \left( \frac{1+c}{2} \right)^{n_b} \sum_{k=0}^{n_a-1} \binom{n_a+n_b-k-2}{n_b-1} \left( \frac{2}{1-c} \right)^k \end{aligned} \quad (21)$$

The integration in Equation 21 is straightforward, because the integral of  $f(y, a, k+1)$  for each index,  $k$ , in the summation contained within  $f_Q$  is equal to one. The frequency of occurrence of mode B is  $\nu_b = 1 - \nu_a$ , and the difference in frequency of occurrence is  $\Delta\nu = \nu_a - \nu_b = 2\nu_a - 1$ . The equation for the difference in mode frequency of occurrence has a simple analytical form when either of  $n_a$  or  $n_b$  is equal to one. When  $n_a = 1$ ,  $\Delta\nu$  is

$$\Delta\nu(c, 1, n_b) = 2 \left( \frac{1+c}{2} \right)^{n_b} - 1. \quad (22)$$

When  $n_b = 1$ ,  $\Delta\nu$  is

$$\Delta\nu(c, n_a, 1) = 1 - 2 \left( \frac{1-c}{2} \right)^{n_a}. \quad (23)$$

The mean linear polarization,  $\mu_L$ , normalized by the mean total intensity, or the mean fractional linear polarization, can be calculated using the expression for the first moment of the Erlang distribution given by Equation 2.



$$\begin{aligned}
\bar{L}(c, n_a, n_b) = \frac{\mu_L}{\mu_I} = & \frac{2}{n_a(1+c) + n_b(1-c)} \left(\frac{1-c}{2}\right)^{n_a} \left(\frac{1+c}{2}\right)^{n_b} \\
& \times \left[ \left(\frac{1+c}{1-c}\right) \sum_{k=0}^{n_a-1} \binom{n_a+n_b-k-2}{n_b-1} \left(\frac{2}{1-c}\right)^k (k+1) \right. \\
& \left. + \left(\frac{1-c}{1+c}\right) \sum_{k=0}^{n_b-1} \binom{n_a+n_b-k-2}{n_a-1} \left(\frac{2}{1+c}\right)^k (k+1) \right] \quad (24)
\end{aligned}$$

The equation for  $\bar{L}$  also has a simple analytical form when either of  $n_a$  or  $n_b$  is equal to one.

$$\bar{L}(c, 1, n_b) = \frac{4}{n_b(1-c) + (1+c)} \left(\frac{1+c}{2}\right)^{n_b+1} - \bar{Q}(c, 1, n_b), \quad (25)$$

$$\bar{L}(c, n_a, 1) = \frac{4}{n_a(1+c) + (1-c)} \left(\frac{1-c}{2}\right)^{n_a+1} + \bar{Q}(c, n_a, 1). \quad (26)$$

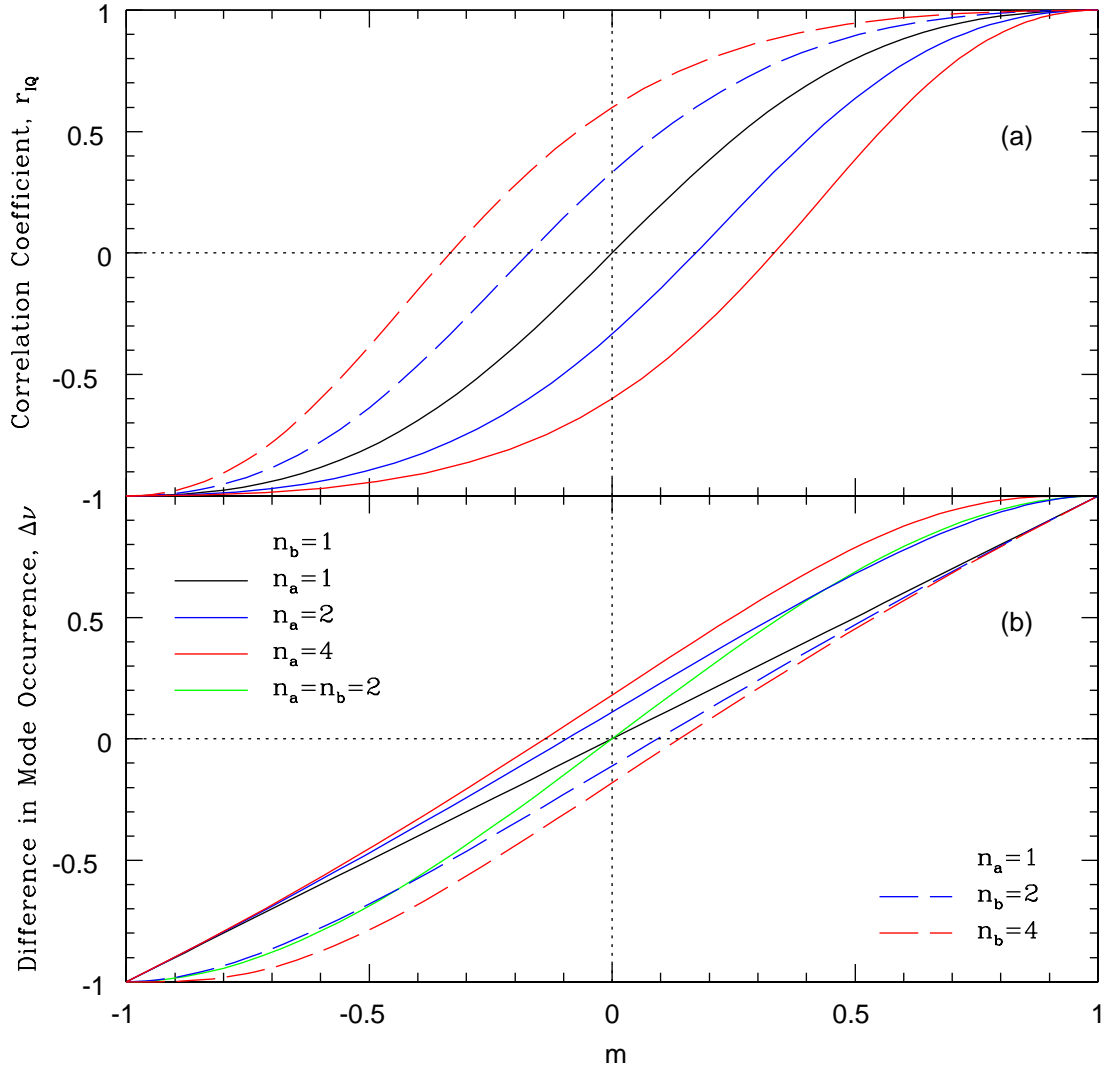
All of the statistical parameters are functions only of  $c$ ,  $n_a$ , and  $n_b$ . They are independent of the values of  $a$  and  $b$ .

### 2.5. Variations in the Statistical Parameters across a Mode Transition

The statistical parameters described in Section 2.4 are average properties calculated at a given pulse phase. They were determined, in part, from the distributions of the Stokes parameters and linear polarization derived in Section 2.3. The variations in the statistical parameters across a mode transition within an average profile are illustrated in this section.

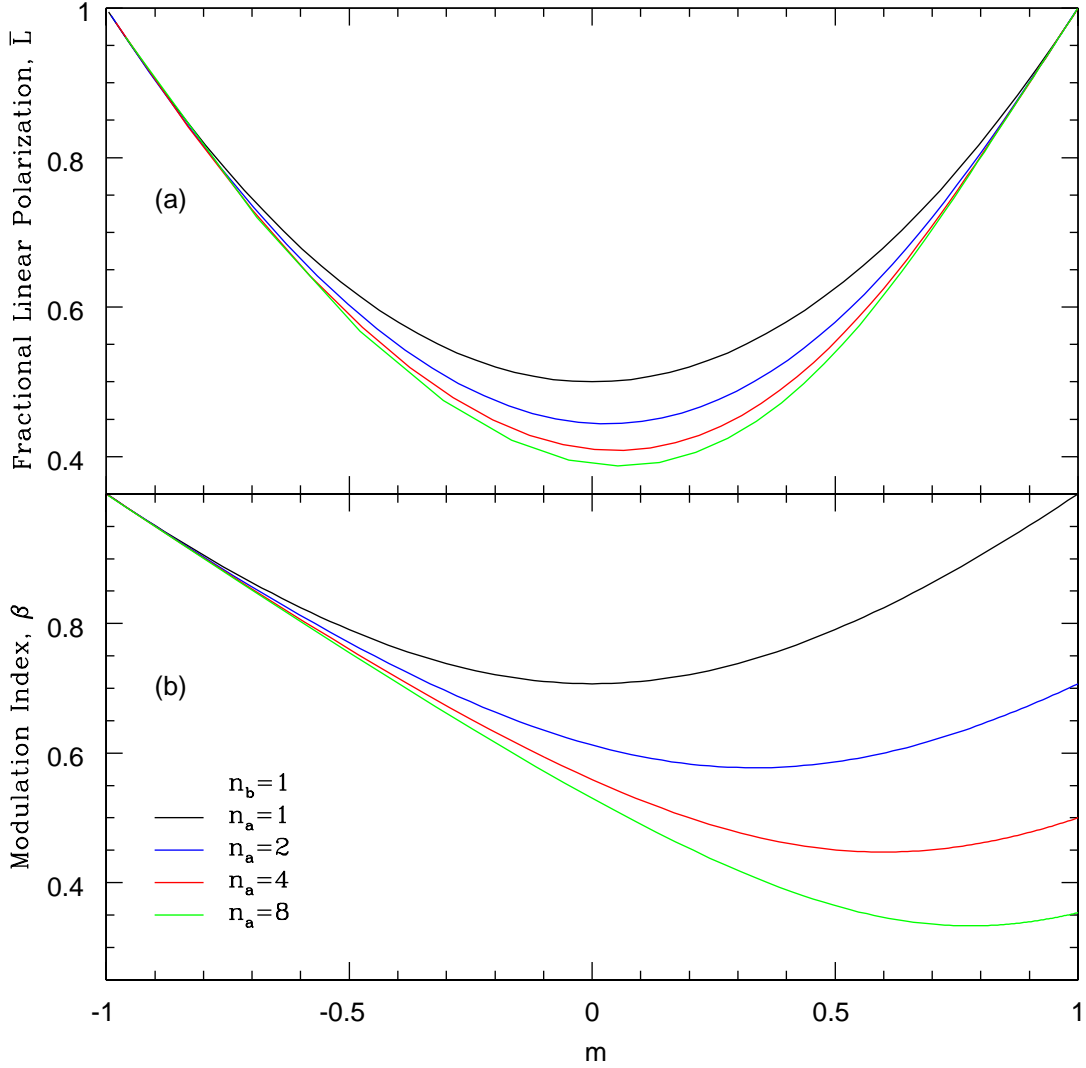
The ratio of the mode mean intensities,  $M$ , changes with variations in the relative scaling of the mode intensity distributions. Changes in  $M$ , or alternatively the parameter  $m$ , with pulse phase drive the transition between the modes. Since  $m$  must change sufficiently to complete the transition, it may be viewed as a proxy for pulse phase over the duration of the transition. The behavior of the statistical parameters across the overall mode transition can be simulated and compared by plotting them as functions of  $m$ . The transition between modes at  $m = 0$  serves as the fiducial point for the comparison.

Figure 1 shows the behavior of  $\Delta\nu$  and  $r_{IQ}$  across a mode transition for different values of  $n_a$  and  $n_b$ . Panel (a) of the figure shows  $r_{IQ}$  calculated from Equation 18. Panel (b) shows  $\Delta\nu$  as calculated from Equations 22 and 23. A transition between modes occurs at  $m = 0$  in both panels of the figure. When  $n_a = n_b$ ,  $\Delta\nu$  and  $r_{IQ}$  are antisymmetric about  $m$ , where they are also equal to zero. The antisymmetry is disrupted when  $n_a \neq n_b$ . The parameters in the figure generally pass through zero at different values of  $m$ . In panel (b), the change in primary mode, as denoted by  $\Delta\nu = 0$ , generally does not coincide with the mode transition. Mode A is the primary mode for values of  $m$  where  $\Delta\nu > 0$ , and mode B is the primary mode where  $\Delta\nu < 0$ . Panel (b) also shows a mode can be the primary over a larger range of  $m$  when  $n_a \neq n_b$  than when  $n_a = n_b$ . Contrary to what one might initially surmise from the model's definitions of I, Q, and  $r_{IQ}$ , the figure shows there are values of  $m$  where mode A (B) is the primary, although the Stokes parameters I and Q are anticorrelated (correlated).



**Figure 1.** The behavior of the I-Q correlation coefficient (a) and difference in mode frequency of occurrence (b) across a mode transition. The solid black, blue, and red lines are drawn for  $n_b = 1$ , with  $n_a$  taking on values of  $n_a = 1, 2, 4$ , respectively. The dashed lines are drawn for  $n_a = 1$ , with  $n_b$  taking on values of  $n_b = 2, 4$ . The solid green line in (b) shows  $\Delta\nu$  when  $n_a = n_b = 2$ . The dependence of  $r_{IQ}$  upon  $m$  for  $n_a = n_b = 2$  is identical to that for  $n_a = n_b = 1$  (see Equation 19).

Figure 2 shows the change in  $\bar{L}$  and  $\beta$  across a mode transition for  $n_b = 1$  and  $n_a = 1, 2, 4$ , and 8. The curves for  $\bar{L}$  shown in panel (a) of the figure were produced from Equation 26. The curves for  $\beta$  in panel (b) were produced using Equation 17. When  $n_a = n_b$ ,  $\bar{L}$  and  $\beta$  are symmetric about  $m = 0$  and pass through minima there. The symmetry of  $\bar{L}$  and  $\beta$  about  $m = 0$  is disrupted when  $n_a \neq n_b$ . Panel (a) shows that the minimum of fractional linear polarization decreases as the sum of  $n_a$  and  $n_b$  increases. The location of the minimum moves to increasing values of  $m$  as  $n_a$  increases. Panel (b) shows that the range of possible values of  $\beta$  is greatest when the order of one mode's distribution is  $n = 1$  and the order of the other distribution is large.



**Figure 2.** Change in fractional linear polarization (a) and modulation index (b) across a mode transition. The curves are drawn for  $n_b = 1$  with  $n_a$  taking on values of  $n_a = 1, 2, 4,$  and  $8$ .

The symmetry properties of the statistical parameters at a mode transition when  $n_a = n_b$  and  $n_a \neq n_b$  are summarized in Table 1.

### 3. ANALYSIS FEATURES

#### 3.1. Detailed Examination of a Mode Transition

The distributions and statistical parameters derived in Sections 2.3 and 2.4 allow a detailed examination of a mode transition when the mode intensities follow different Erlang distributions. A transition from mode A to mode B is illustrated in Figure 3 when  $n_a = 2$  and  $n_b = 1$ . Panel (a) of the figure shows the I-Q correlation coefficient, normalized mean of the Stokes parameter Q, and the difference in mode frequency of occurrence as functions of  $m$ . Panel (b) shows the modulation index and normalized mean of the linear polarization. At point A in panel (a) of the figure,  $m = c = 1$  and

**Table 1.** Symmetry Properties of Statistical Parameters across a Mode Transition

Mode Erlang Order	$n_a = n_b$	$n_a \neq n_b$
Normalized Stokes Q, $m = \bar{Q}$	Antisymmetric	Antisymmetric
Difference in mode occurrence, $\Delta\nu$	Antisymmetric	Asymmetric
I-Q correlation coefficient, $r_{IQ}$	Antisymmetric	Asymmetric
Normalized linear polarization, $\bar{L}$	Symmetric	Asymmetric
Modulation index, $\beta$	Symmetric	Asymmetric
Mean intensity ratio, $M$	$M = C$	$M \neq C$
Normalized Stokes Q, $m$	$m = c$	$m \neq c$

the emission is comprised solely of mode A. The emission is completely polarized, and the Stokes parameters I and Q are completely correlated. The modulation index is equal to that of mode A ( $\beta = 1/\sqrt{n_a}$ ). The statistical parameters decrease as  $m$ , or  $c$ , decreases. At point R in the figure,  $C = n_a/n_b$ , and  $c$  is

$$c = \frac{n_a - n_b}{n_a + n_b}. \quad (27)$$

The values of  $m$  and  $r_{IQ}$  at point R are always

$$m = \frac{n_a^2 - n_b^2}{n_a^2 + n_b^2}, \quad (28)$$

$$r_{IQ} = \frac{n_a^3 - n_b^3}{n_a^3 + n_b^3}. \quad (29)$$

For the example shown in the figure, the correlation coefficient happens to equal the difference in mode frequency of occurrence, which is not true in general. From Equation 23 when  $n_b = 1$ ,  $\Delta\nu$  at point R is

$$\Delta\nu = 1 - 2 \left( \frac{1}{1 + n_a} \right)^{n_a}. \quad (30)$$

Decreasing the value of  $m$  further, the normalized mean of Stokes Q and the correlation coefficient are equal to one another at point E in the figure, where  $C = 1$  and  $c = 0$ .

$$m = \bar{Q} = r_{IQ} = \frac{n_a - n_b}{n_a + n_b} \quad (31)$$

The modulation index is always minimum at this location, where it is  $\beta = 1/\sqrt{n_a + n_b}$ . From Equation 23, the difference in mode frequency of occurrence at point E is

$$\Delta\nu = 1 - 2^{1-n_a}. \quad (32)$$

The correlation coefficient is equal to zero when the mode variances are equal to one another. This occurs at point G in the figure, where  $C = \sqrt{n_b/n_a}$  and  $c = -m$ .

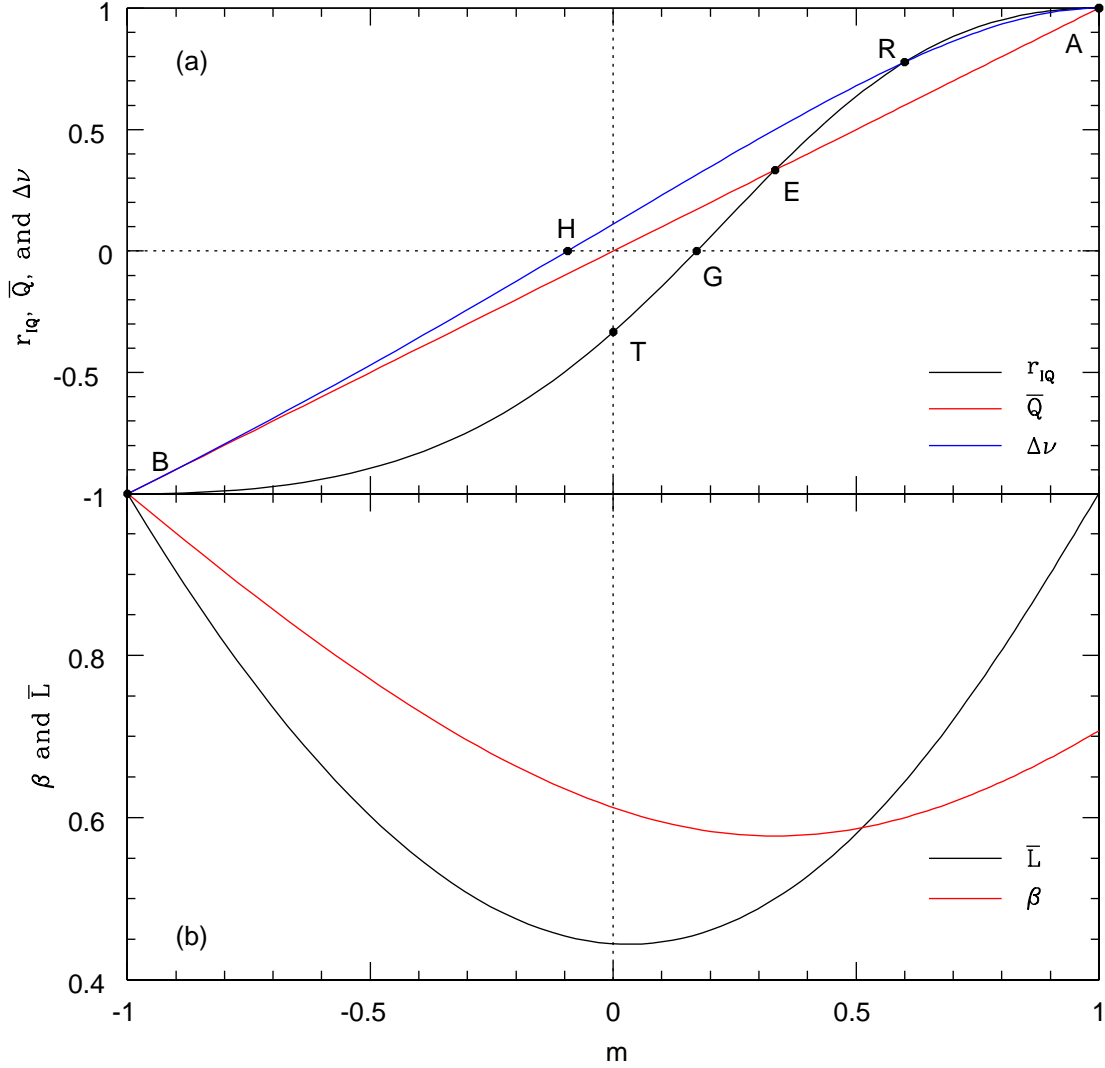


**Figure 3.** Variations in the statistical parameters across a mode transition when  $n_a = 2$  and  $n_b = 1$ . Panel (a) shows the change in I-Q correlation coefficient ( $r_{IQ}$ ), normalized Stokes parameter Q ( $\bar{Q}$ ), and difference in mode frequency of occurrence ( $\Delta\nu$ ) with the parameter  $m$ . Panel (b) shows the dependence of the normalized linear polarization ( $\bar{L}$ ) and modulation index ( $\beta$ ) upon  $m$ . Decreasing the value of  $m$  drives the transition from mode A to mode B. See the text and Table 2 for explanations of the points labeled in the figure.

$$c = -m = \frac{\sqrt{n_b} - \sqrt{n_a}}{\sqrt{n_b} + \sqrt{n_a}} \quad (33)$$

The Stokes parameters I and Q are positively correlated for values of  $m$  to the right of point G, and are negatively correlated for values of  $m$  to the left of it. Mode A remains the primary mode, as indicated by  $\Delta\nu > 0$ , and  $\bar{Q} = m$  remains positive despite the onset of the anticorrelation. The difference in mode frequency of occurrence at G is

**Table 2.** Values of Select Statistical Parameters across a Mode Transition

Point	Description	$c$	$C$	$m = \bar{Q}$	$r_{IQ}$	$\beta$
A	Mode A only	1	$\infty$	1	1	$\frac{1}{\sqrt{n_a}}$
R	Mode A dominated	$\frac{n_a - n_b}{n_a + n_b}$	$\frac{n_a}{n_b}$	$\frac{n_a^2 - n_b^2}{n_a^2 + n_b^2}$	$\frac{n_a^3 - n_b^3}{n_a^3 + n_b^3}$	$\frac{\sqrt{n_a^3 + n_b^3}}{n_a^2 + n_b^2}$
E	Minimum modulation	0	1	$\frac{n_a - n_b}{n_a + n_b}$	$\frac{n_a - n_b}{n_a + n_b}$	$\frac{1}{\sqrt{n_a + n_b}}$
G	No I-Q correlation	$\frac{\sqrt{n_b} - \sqrt{n_a}}{\sqrt{n_b} + \sqrt{n_a}}$	$\sqrt{\frac{n_b}{n_a}}$	$\frac{\sqrt{n_a} - \sqrt{n_b}}{\sqrt{n_a} + \sqrt{n_b}}$	0	$\frac{\sqrt{2}}{\sqrt{n_a} + \sqrt{n_b}}$
T	Mode transition	$\frac{n_b - n_a}{n_b + n_a}$	$\frac{n_b}{n_a}$	0	$\frac{n_b - n_a}{n_b + n_a}$	$\frac{1}{2} \sqrt{\frac{n_a + n_b}{n_a n_b}}$
B	Mode B only	-1	0	-1	-1	$\frac{1}{\sqrt{n_b}}$

$$\Delta\nu = 1 - 2 \left( \frac{\sqrt{n_a}}{1 + \sqrt{n_a}} \right)^{n_a}. \quad (34)$$

The transition between modes occurs at point T in the figure, where the mode mean intensities are equal and  $\bar{Q} = m = 0$ . The value of the parameter  $C$  at point T is  $C = n_b/n_a$ , and  $c$  is equal to the I-Q correlation coefficient.

$$c = r_{IQ} = \frac{n_b - n_a}{n_b + n_a}. \quad (35)$$

The fractional linear polarization goes through a broad minimum between points G and T, but its minimum (at  $m = 0.033$  in the figure) does not coincide with T ( $m = 0$ ). From Equation 26, the mean fractional linear polarization at T is

$$\bar{L} = \left( \frac{n_a}{1 + n_a} \right)^{n_a}. \quad (36)$$

The difference in frequency of occurrence at point T is

$$\Delta\nu = 1 - 2 \left( \frac{n_a}{1 + n_a} \right)^{n_a}. \quad (37)$$

Since  $\Delta\nu$  is generally not equal to zero at T, mode A unexpectedly remains the primary mode as  $\bar{Q}$  passes from positive to negative.

The modes occur with equal frequency, and the primary mode changes from mode A to mode B, at point H in the figure, where  $\Delta\nu = 0$  (or  $\nu_a = \nu_b = 1/2$ ). When  $n_b = 1$ , the change between primary modes occurs at

$$c = 1 - 2 \frac{n_a - 1}{n_a}. \quad (38)$$

This value of  $c$  causes  $y = 0$  to be the median of the Stokes Q distribution (see Equation 6). Mode A is the primary mode for all values of  $m$  to the right of point H in the figure, and mode B is the primary for all values of  $m$  to the left of it. The region between points T and H has interesting

implications for the polarization's average properties. In this region of the figure,  $\bar{Q}$  is negative, but mode A is the primary mode, because  $\Delta\nu > 0$ . Since the Stokes parameters Q and V are proportional to one another when the OPMs are elliptically polarized (see Equation 10),  $\bar{Q}$  is a proxy for circular polarization, which in turn means the sense of the circular polarization between T and H on average is that of mode B (negative), although the PA is predominantly that of mode A.

The emission is comprised solely of mode B at point B, where  $m = c = -1$ . The emission is completely polarized and the Stokes parameters I and Q are completely anticorrelated. The modulation index is equal to that of mode B ( $\beta = 1/\sqrt{n_b}$ ).

The values of  $c$ ,  $C$ ,  $m$ ,  $r_{IQ}$  and  $\beta$  at each of the points A, R, E, G, T, and B in the mode transition are summarized in Table 2. They are dependent only on the values of  $n_a$  and  $n_b$  and are independent of the scaling factors  $a$  and  $b$ . The points R, E, G, T, and H merge at  $m = c = 0$  when  $n_a = n_b$ .

The distributions of fractional linear polarization at each of the points R, E, G, T, and H are shown in Figure 4. The distributions were calculated from Equation 12 with  $\chi_o = 0$ . The distribution at point R is shown by the magenta line in the figure. The slope of the distribution is generally positive for all values of  $z$ . Many data samples are highly, if not completely, polarized because the intensity of mode B, owing to its exponential distribution, is frequently very low, whereas the intensity of mode A is rarely so. The distribution at point E in this specific case (the horizontal black line in the figure) is uniform, demarcating a change in the general slope of the distributions from positive to negative as  $c$  continues to decrease. Despite the emission's random polarization implied by the distribution at this location, it is still dominated by mode A with a frequency of occurrence of  $\nu_a = 3/4$  (or  $\Delta\nu = 1/2$  from Equation 23). The distributions at points G, T, and H (the green, red, and blue lines, respectively) are similar in form with generally negative slopes over the full range of  $z$ . The intercepts of the distributions at  $z = 0$  initially increase with decreasing  $c$ , reaching a maximum at point T. Thereafter, the intercepts decrease as mode B becomes the primary mode. The distribution at  $c = -0.8$  ( $m = -0.636$ , the cyan line) was arbitrarily selected to illustrate the distribution when mode B is the primary mode. The shape of the distribution there is quite different from when mode A is the primary. The distribution develops a peak as the value of  $c$  decreases. Although many data samples in the distribution are highly polarized, they are not completely polarized, because the intensity of mode A is never equal to zero, unless it is completely absent (i.e. when  $c = m = -1$ ).

### 3.2. Modulation and Depolarization

The effectiveness of superposed OPMs in depolarizing the emission and the relationship between depolarization and intensity modulation can be explored with the equations for  $\bar{L}$  and  $\beta$ . Panel (b) of Figure 5 shows  $\bar{L}$  for different values of  $n_a$  and  $n_b$  with their sum held constant at  $n_a + n_b = 8$ . The smallest value of  $\bar{L}$  (the most depolarization) occurs when  $n_a = n_b = 4$  at  $m = 0$ . For each pair of  $n_a$  and  $n_b$  in the panel, the minimum value of the modulation index is always  $\beta = 1/\sqrt{8}$ . As  $n_a$  increases at the expense of  $n_b$ , the minimum of  $\bar{L}$  increases with respect to  $\bar{L}(0, 4, 4)$  at slightly increasing values of  $m$ . The conclusion to be drawn from panel (b) is, for a fixed value of  $n_a + n_b$ , the depolarization is maximum when the distributions of the mode intensities are identical (i.e. when  $n_a = n_b$  and  $a = b$ ). Panel (a) of the figure shows  $\bar{L}$  when  $n_a = n_b = n$  for different values of  $n$ . The magenta curve is  $\bar{L}$  derived for Gaussian mode intensities (see the discussion of Equation 45 in Section 3.3). The curves are symmetric about  $m = 0$  where  $\bar{L}$  is minimum. From Equation 24, the value of  $\bar{L}$  at  $m = c = 0$  is

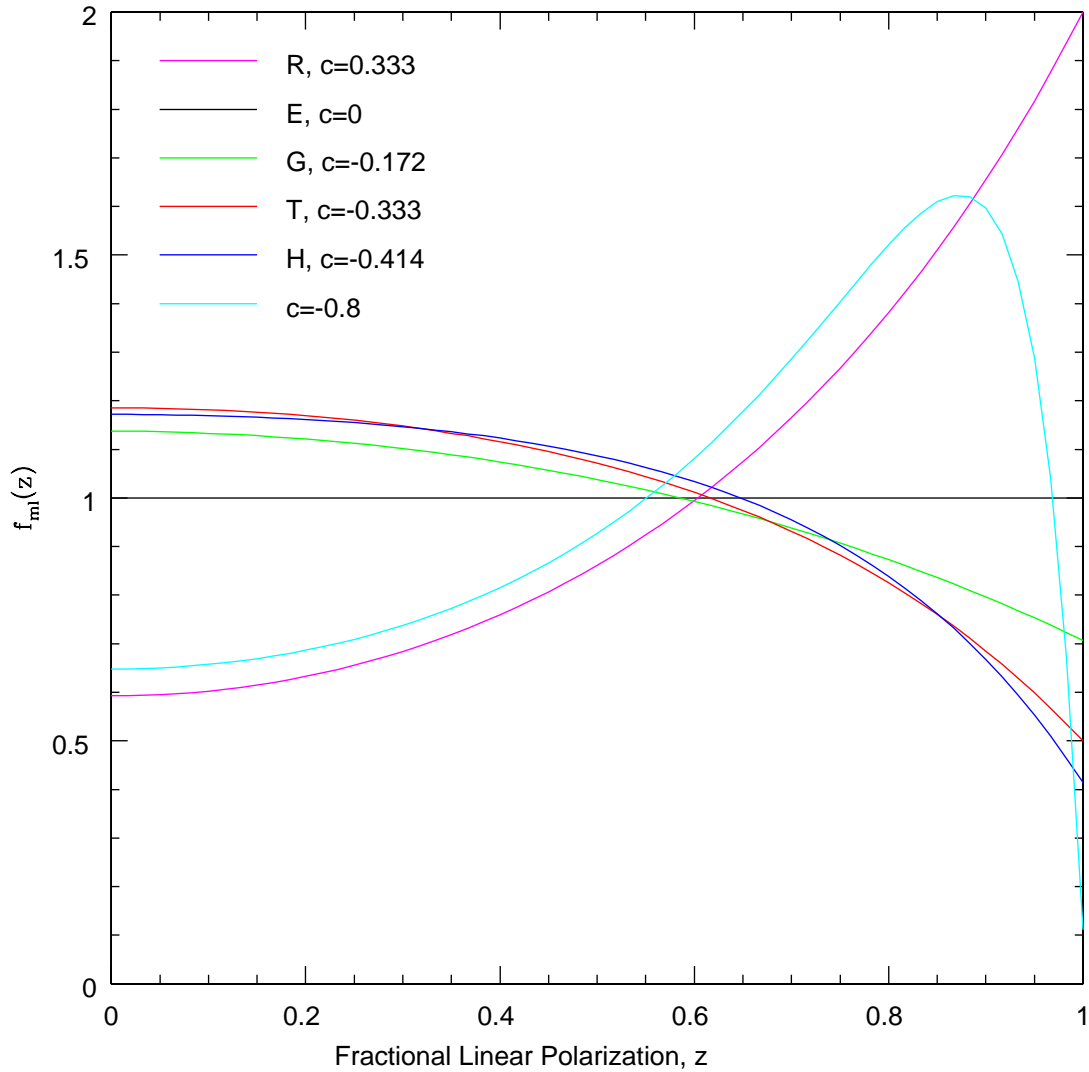


**Figure 4.** The distributions of fractional linear polarization at different points within a mode transition. The points correspond to those labeled R, E, G, T, and H in Figure 3 and Table 2. The distribution at  $c = -0.8$  is also shown for comparison. The values of  $n_a$ ,  $n_b$ , and  $\chi_o$  used to produce the figure are  $n_a = 2$ ,  $n_b = 1$ , and  $\chi_o = 0$ .

$$\bar{L}(0, n, n) = \frac{1}{n2^{2n-1}} \frac{(2n-1)!}{(n-1)!^2}, \quad (39)$$

and the modulation index is  $\beta = 1/\sqrt{2n}$ . The additional conclusion to be drawn from panel (a) of the figure is the mean fractional linear polarization is minimum when the modulation index is small ( $n$  is large); the less the mode intensities fluctuate, the more depolarization will occur. Equation 39 then represents a lower limit on the fractional linear polarization that can be attained through superposed OPMs as a function of  $n$ . The limit on  $\bar{L}$  is related to modulation index through  $n$ . The limit as a function of  $\beta$  is shown by the open circles in Figure 6 for  $1 \leq n \leq 40$ . The solid line in the figure is



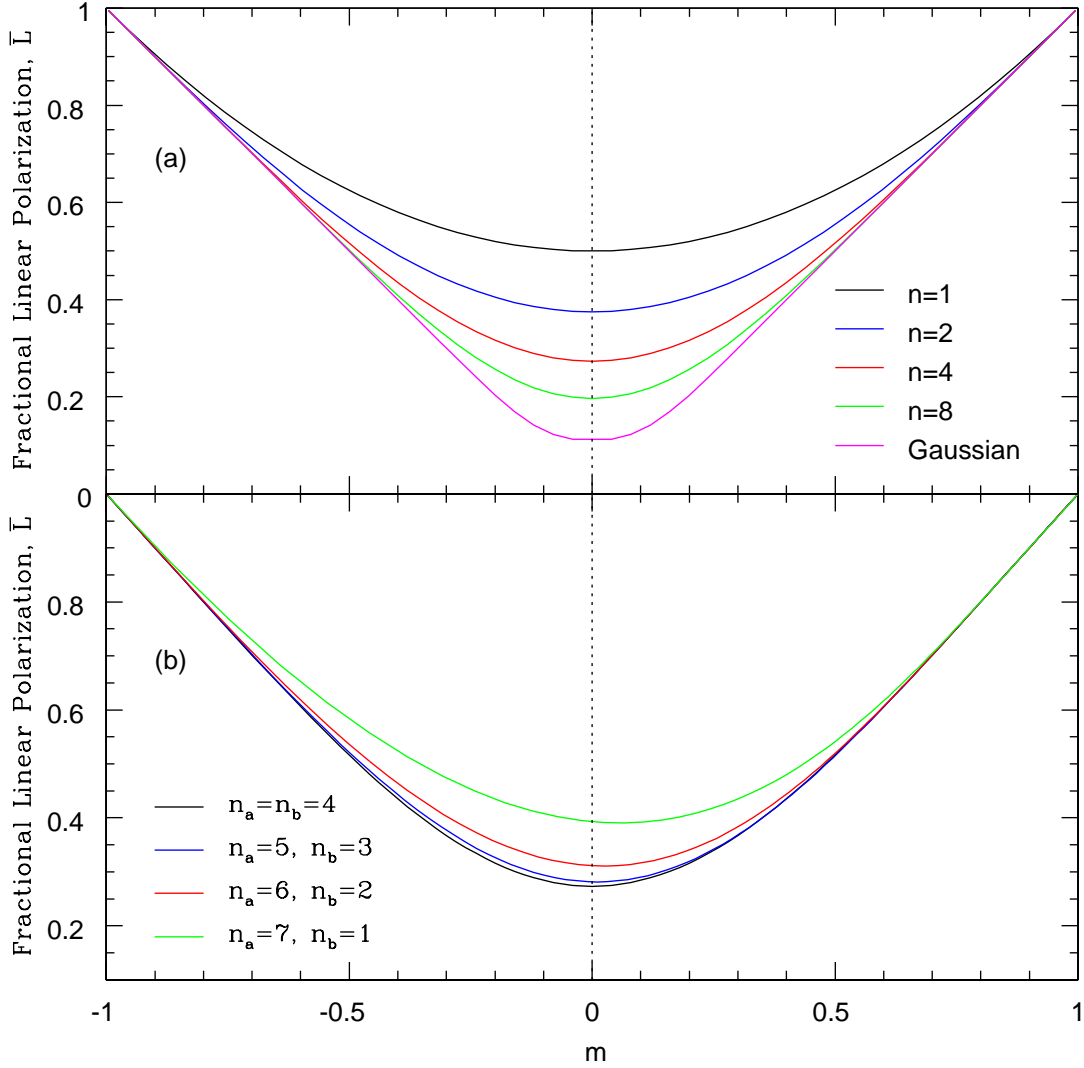


**Figure 5.** Mean fractional linear polarization,  $\bar{L}$ , for different values of  $n_a$  and  $n_b$ . Panel (a) shows  $\bar{L}$  when  $n_a = n_b = n$ , for  $n = 1, 2, 4$ , and  $8$  (Equation 24). The lower envelope in the panel is  $\bar{L}$  derived from Gaussian fluctuations in the mode intensities (Equation 45). Panel (b) shows  $\bar{L}$  when the sum of  $n_a$  and  $n_b$  remains constant at  $n_a + n_b = 8$ .

the same limit derived from Gaussian fluctuations in mode intensities, and is discussed in Section 3.3 (see Equation 46). The figure shows the fractional linear polarization remains high ( $\bar{L} = 1/2$ ) when the modulation index is large ( $\beta = 1/\sqrt{2}$ ).

### 3.3. Statistical Parameters and Distributions for Gaussian Mode Intensities

As the order of the Erlang distributions of mode intensities becomes very large, the various distributions and statistical parameters derived from the statistical model should resemble those derived from Gaussian-distributed mode intensities. The distributions and parameters arising from Gaussian fluctuations were derived in MS; however, they were not presented as functions of  $m$  in that

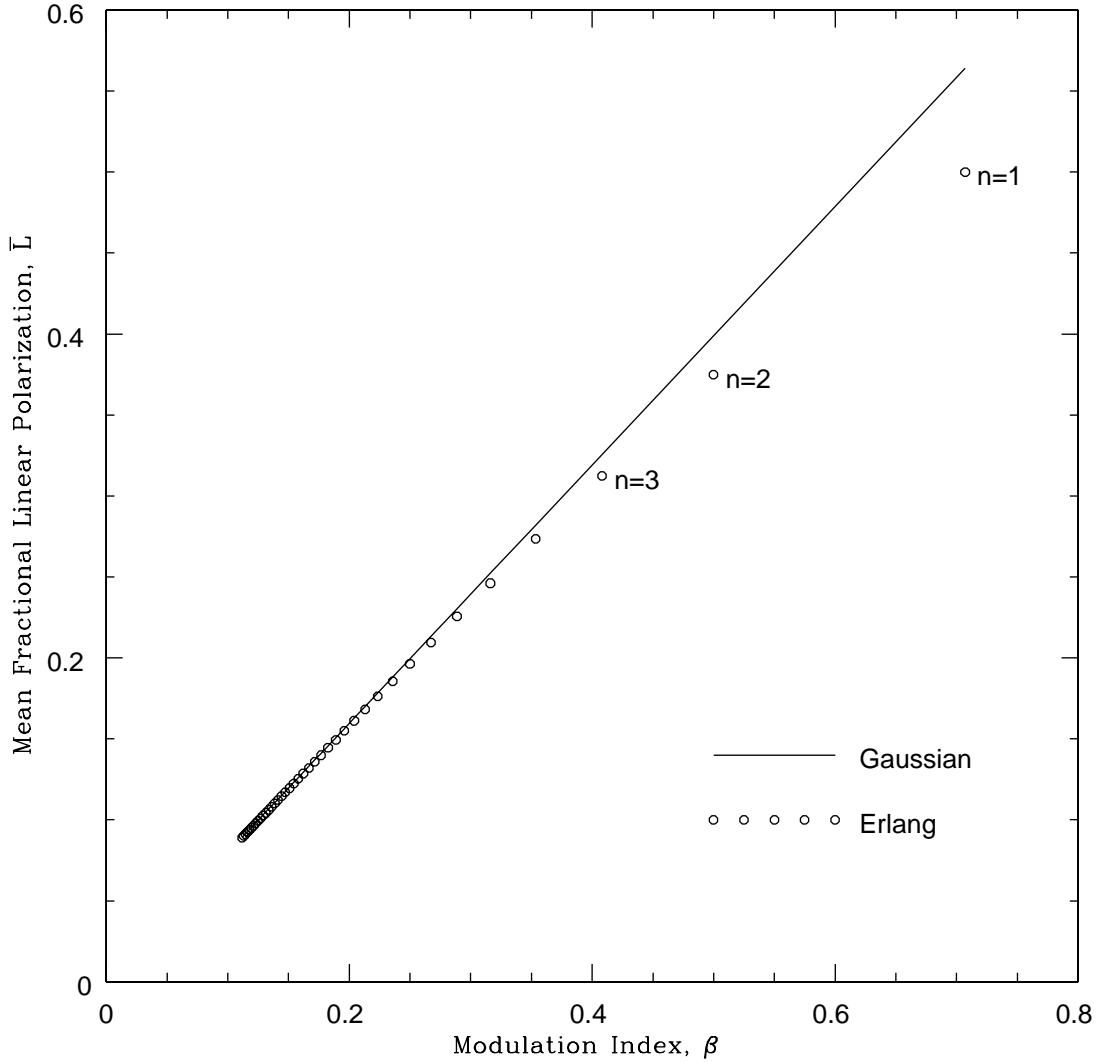


**Figure 6.** Lower limit on the fractional linear polarization,  $\bar{L}$ , that can be attained through superposed OPMs as a function of modulation index,  $\beta$ . The open circles denote the limit when the mode intensities are Erlang RVs with  $1 \leq n \leq 40$  (Equation 39). The solid line is the limit derived when the mode intensities are Gaussian RVs extrapolated to large values of  $\beta$  (Equation 46).

original implementation of the model. The distributions and parameters written in terms of  $m$  are summarized here to facilitate their comparison with what was derived from Erlang mode intensities.

When the mode intensities are Gaussian RVs, the normalized Stokes parameter  $Q$  is  $\bar{Q} = m$ , and the I-Q correlation coefficient is always zero,  $r_{IQ} = 0$  (MS). The modulation index is constrained to be

$$\beta(m) \leq \frac{1 - |m|}{5\sqrt{2}}. \quad (40)$$

The constraint on  $\beta$  arises from how the statistical model was implemented in MS. The standard deviations of the mode intensities,  $\sigma$ , were held constant and equal to make the Stokes parameters I and Q independent of one another. The parameter  $m$  (or  $M$ ) was then varied by effectively holding the mean intensity of the secondary mode constant and varying the mean of the primary mode. The mean intensity of the secondary mode must have a minimum value of about  $5\sigma$  to ensure its intensity is always nonnegative.

The frequency of occurrence of mode A for Gaussian mode intensities is given by Equation 15 of MS

$$\nu_a = \frac{1}{2} \left[ 1 + \operatorname{erf} \left( \frac{\mu_Q}{\sigma_Q \sqrt{2}} \right) \right], \quad (41)$$

where  $\operatorname{erf}(x)$  is the error function,  $\mu_Q$  is the mean of the Stokes parameter Q, and  $\sigma_Q$  is its standard deviation. As with Equation 40, Equation 41 assumes the standard deviations of the mode intensities are equal, which in turn means the standard deviations of the Stokes parameters I and Q are also equal,  $\sigma_Q = \sigma_I = \sigma\sqrt{2}$ . Recognizing that  $\mu_Q = m\mu_I$  and  $\beta = \sigma_I/\mu_I$ , the equation can be rewritten in terms of  $m$  and  $\beta$  as

$$\nu_a(m, \beta) = \frac{1}{2} \left[ 1 + \operatorname{erf} \left( \frac{m}{\beta\sqrt{2}} \right) \right], \quad (42)$$

The difference in mode frequency of occurrence is

$$\Delta\nu(m, \beta) = \operatorname{erf} \left( \frac{m}{\beta\sqrt{2}} \right). \quad (43)$$

The frequencies of occurrence for mode A derived from Gaussian and Erlang fluctuations in mode intensities are compared in Figure 7. The dependence of  $\nu_a$  upon  $m$  for Gaussian fluctuations was calculated from Equation 42 using Equation 40 for the functional dependence of  $\beta$  upon  $m$ . Equation 21 was used to calculate  $\nu_a$  for Erlang fluctuations when  $n_a = n_b = n$ . The different values of  $n$  used to calculate  $\nu_a$  are annotated in the figure. The figure shows that  $\nu_a$  for Erlang fluctuations approaches that for Gaussian fluctuations as the value of  $n$  increases, as expected from the central limit theorem. Each example of  $\nu_a$  in the figure is antisymmetric about  $m = 0$ , because the mode intensity distributions are identical to one another in each case. The frequency of occurrence changes rapidly near  $m = 0$  for Gaussian intensity fluctuations, but changes more gradually over  $m$  for Erlang fluctuations. When  $n = 1$ , the mode frequency of occurrence varies linearly with  $m$ ,  $\nu_a = (1 + m)/2$  (M22). When  $n$  is large, a small change in  $m$  near  $m = 0$  can result in a large change in  $\nu_a$ . Since the modulation index of an Erlang distribution is generally larger than that for a Gaussian distribution, one may infer that rapid changes in  $\nu_a$  occur where the modulation index is small, and more gradual changes occur where the modulation index is large.

The mean of the linear polarization for Gaussian fluctuations in mode intensities is given by Equation 13 of MS.

$$\mu_L = \sigma_Q \sqrt{\frac{2}{\pi}} \exp \left( -\frac{\mu_Q^2}{2\sigma_Q^2} \right) + \operatorname{erf} \left( \frac{\mu_Q}{\sigma_Q \sqrt{2}} \right) \mu_Q. \quad (44)$$

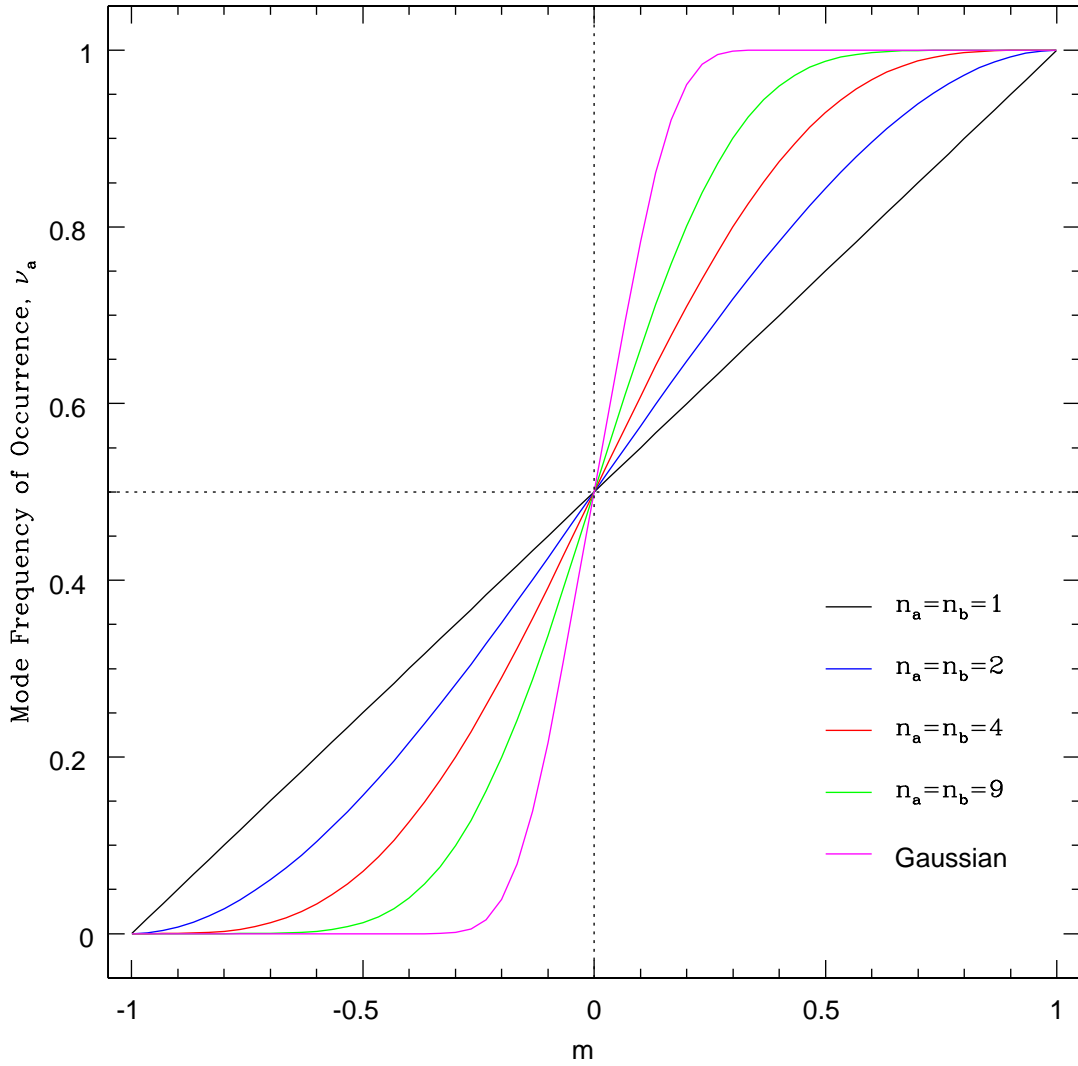


**Figure 7.** Behavior of the mode frequency of occurrence,  $\nu_a$ , at a mode transition when the mode intensities are Erlang (Equation 21) and Gaussian (Equation 42) RVs. The transition occurs at  $m = 0$ . The values of  $n$  used for the Erlang distributions are annotated in the figure.

Dividing  $\mu_L$  by the mean total intensity and rewriting the equation in terms of  $m$  and  $\beta$  gives the normalized mean of the linear polarization.

$$\bar{L}(m, \beta) = \beta \sqrt{\frac{2}{\pi}} \exp\left(-\frac{m^2}{2\beta^2}\right) + \operatorname{erf}\left(\frac{m}{\beta\sqrt{2}}\right) m. \quad (45)$$

Equation 45 with  $\beta$  given by Equation 40 is shown by the magenta curve in panel (a) of Figure 5. The first term in the equation is the contribution of the polarization fluctuations to  $\bar{L}$ , and the second term is the contribution of the persistent polarization to  $\bar{L}$ . The equation shows that  $\bar{L}$  can never be zero when the polarization fluctuates (i.e. when  $\beta \neq 0$ ). Since  $m = 0$  at an OPM transition for Gaussian mode intensities, the fractional linear polarization at the transition is directly proportional

to the modulation index,  $\bar{L} = \beta\sqrt{2/\pi}$ , and is small where  $\beta$  is also small. This is the smallest the fractional linear polarization can be when the mode intensities are Gaussian RVs. The asymptotic behavior of  $\bar{L}$  at large values of  $n$  for Erlang mode intensities can be determined by setting the limit given by Equation 39 equal to  $\bar{L}$  calculated for Gaussian mode intensities. Since the modulation index for Erlang mode intensities is  $\beta = 1/\sqrt{2n}$  when  $m = 0$ , the limit on  $\bar{L}$  at large values of  $n$  is

$$\bar{L} = \beta \left( \frac{2}{\pi} \right)^{1/2} = \left( \frac{1}{n\pi} \right)^{1/2}. \quad (46)$$

Equation 46 is shown by the solid line in Figure 6. The figure shows the minimum in fractional linear polarization derived from Gaussian fluctuations in mode intensities is in good agreement with the result obtained from Erlang fluctuations when  $n$  is large. The minimum for true Gaussian fluctuations is applicable only for  $\beta \leq 1/(5\sqrt{2})$  (or  $n \geq 25$ ). The line has been extended in the figure to include  $n = 1$  to provide a full comparison between the two results.

When the mode intensities are Gaussian RVs, the distributions of the Stokes parameters are also Gaussian (MS). The distribution of linear polarization is the sum of two Gaussians with equal variances. Their means are also equal in magnitude, but with opposite signs (see Equation 27 of MS). The distribution of fractional linear polarization is given by Equation 16 of MS. Reparameterizing that equation in terms of  $m$  and  $\beta$ , and accounting for the ellipticity of the modes' polarization, gives

$$fml(z, m, \beta, \chi_o) = \frac{1}{\beta\sqrt{2\pi}} \frac{\cos(2\chi_o)}{(z^2 + \cos^2(2\chi_o))^{3/2}} \left\{ (\cos(2\chi_o) + mz) \exp \left[ -\frac{(z - m \cos(2\chi_o))^2}{2\beta^2(z^2 + \cos^2(2\chi_o))} \right] \right. \\ \left. + (\cos(2\chi_o) - mz) \exp \left[ -\frac{(z + m \cos(2\chi_o))^2}{2\beta^2(z^2 + \cos^2(2\chi_o))} \right] \right\}. \quad (47)$$

The distribution of fractional circular polarization is

$$fmv(z, m, \beta, \chi_o) = \frac{\sin(2\chi_o)}{\beta\sqrt{2\pi}} \frac{\sin(2\chi_o) + mz}{(z^2 + \sin^2(2\chi_o))^{3/2}} \exp \left[ -\frac{(z - m \sin(2\chi_o))^2}{2\beta^2(z^2 + \sin^2(2\chi_o))} \right]. \quad (48)$$

The distribution is approximately Gaussian with a mean of  $m \sin(2\chi_o)$  and a standard deviation of  $\beta \sin(2\chi_o)$ . The distributions of fractional polarization for Gaussian and Erlang fluctuations in mode intensities are compared in Figures 8 and 9 when the conditions used to derive the equations for them are satisfied. This occurs when the Erlang mode intensities are identically distributed ( $n_a = n_b \gg 1$  and  $m = 0$ ) or when their variances are equal (i.e. when  $r_{IQ} = 0$ ), as at point G in Figure 3 and Table 2. The modulation index of the total intensity resulting from Gaussian fluctuations must also satisfy  $\beta \leq 1/(5\sqrt{2})$ . The parameters used to calculate the distributions are annotated in each panel of the figures. The distributions resemble one another, which is noteworthy considering the substantial differences between their functional forms.

Equations 42, 43, 45, 47, and 48 are written as functions of  $m$  and  $\beta$  for conciseness and to indicate how the statistical parameters and fractional polarization distributions are influenced by them, but with the understanding that  $m$  and  $\beta$  are not independent and follow the constraint stipulated by Equation 40.

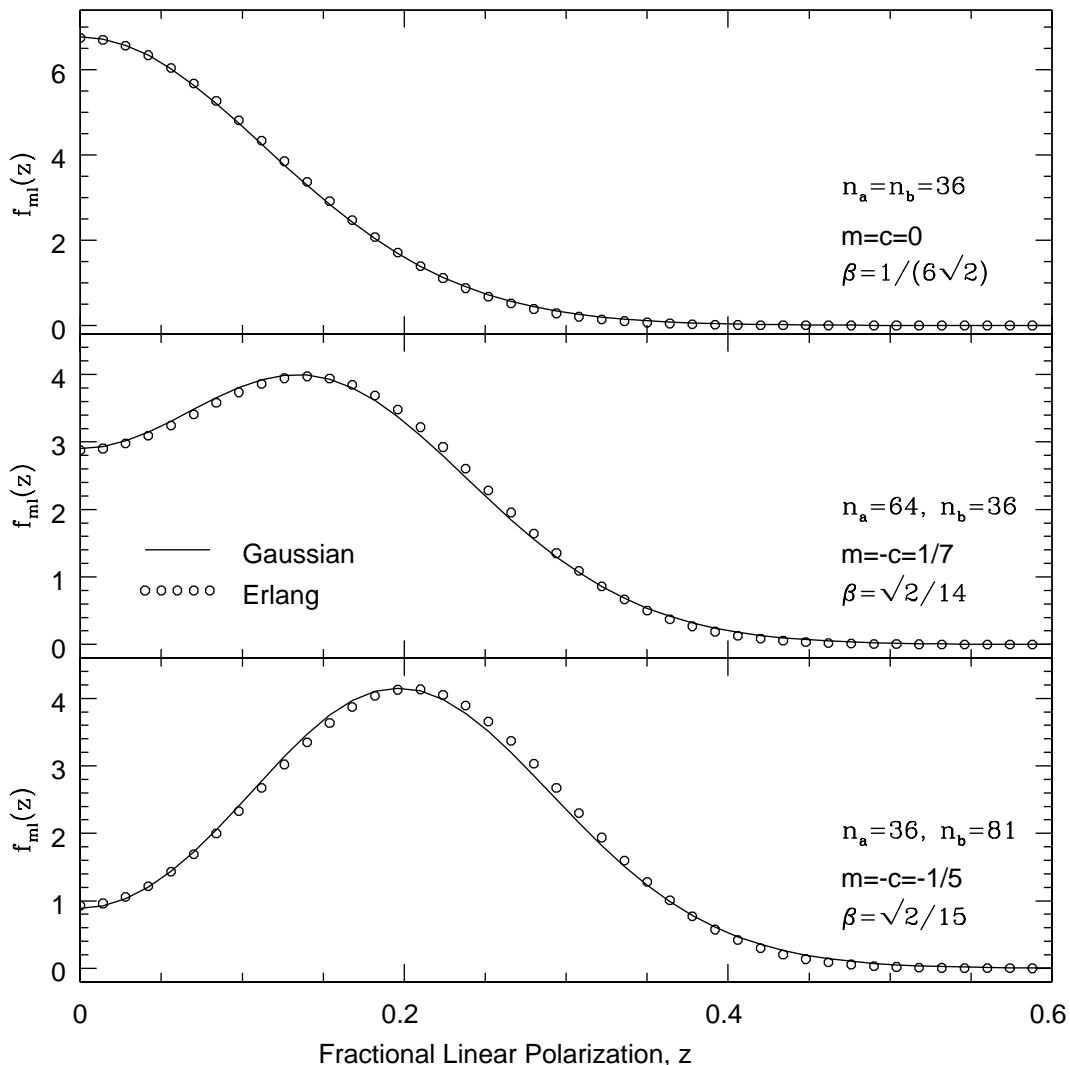


**Figure 8.** Comparison of distributions of fractional linear polarization when the fluctuations in mode intensities are Gaussian and Erlang RVs. The distributions resulting from Gaussian fluctuations (Equation 47) are shown by the solid lines, and the distributions resulting from Erlang fluctuations (Equation 12) are denoted by open circles. The values of  $n_a$ ,  $n_b$ ,  $c$ , and  $\beta$  used to determine the distributions are annotated in each panel of the figure. The value of the ellipticity angle used in the figure is  $\chi_o = 0$ .

## 4. DISCUSSION

### 4.1. Summary Comments on the Analysis

The MS statistical model recognizes and incorporates the stochastic nature of pulsar radio emission and the tendency of its polarization to randomly switch between orthogonally polarized states. The model can replicate observed distributions of the Stokes parameters, linear polarization, and polarization position angle at a given pulse phase (MS, M22). It predicts polarization fluctuations have a preferred orientation in the Poincaré sphere (M04). The orientation becomes more apparent as the modulation index increases. The implementation of the model in this analysis, where the mode

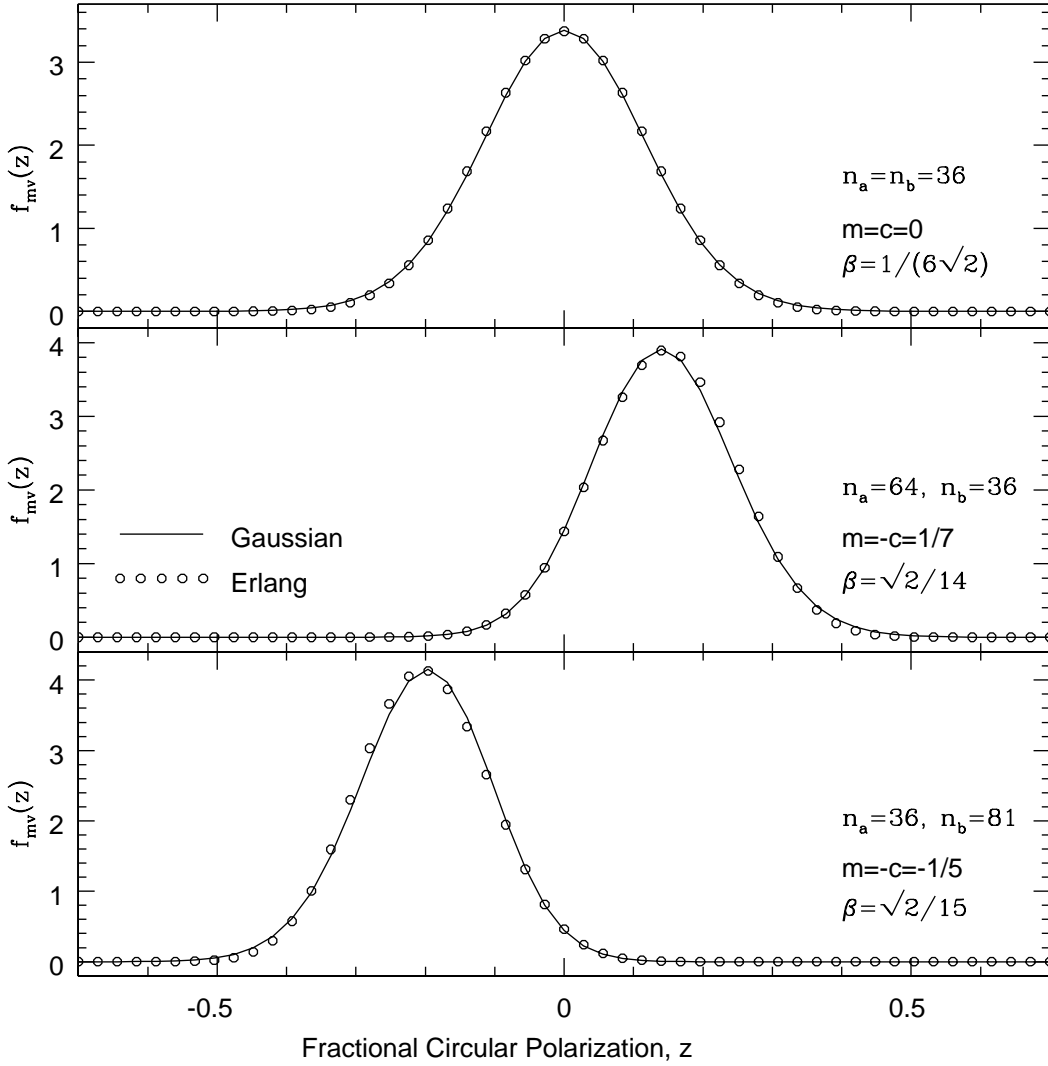


**Figure 9.** Comparison of distributions of fractional circular polarization when the fluctuations in mode intensities are Gaussian and Erlang RVs. The distributions resulting from Gaussian fluctuations (Equation 48) are shown by the solid lines, and the distributions resulting from Erlang fluctuations (Equation 11) are denoted by open circles. The value of the ellipticity angle used in the figure is  $\chi_o = \pi/4$ .

intensities are assumed to be Erlang RVs, is the general version of the specific cases considered in MS and M22. The analysis in M22 represents one extreme of the general case, where the mode intensity fluctuations are modeled as exponential RVs ( $n = 1$ ). The analysis in MS is the other extreme, where the fluctuations are modeled as Gaussian RVs ( $n \gg 1$ ). All intervening values of the order of the Erlang intensity distributions,  $n$ , can be accommodated by the analysis presented here.

A pulse phase-resolved transition between the polarization modes in an average profile can be modeled by virtue of the analysis. The modeling is enabled by the realization that the ratio of the mode mean intensities, as represented by the parameter  $m$ , drives the transition. Since  $m$  must vary with pulse phase,  $\phi$ , to complete the transition,  $m$  is a proxy for  $\phi$  over the transition's duration. The

simplest relationship between  $m$  and  $\phi$  is they are proportional to one another (see, e.g., McKinnon 2003).

The analysis allows an investigation into how mode intensities of different statistical character might affect the observed polarization. When the mode intensities are identically distributed, the mean fractional linear polarization and modulation index are symmetric about a mode transition in an average profile. The symmetry is disrupted when the mode intensity distributions are different. The latter scenario may manifest itself in seemingly anomalous ways, such as a minimum in the fractional linear polarization that does not coincide with the mode transition, or the prevailing sense of the circular polarization in an average profile is that of one mode although the PA histogram at the same pulse phase indicates the other mode is occurring more frequently.

The analysis also posits that the fluctuations in mode intensities at least contribute to, or may completely determine, the overall modulation of the emission. The statistical character of the mode intensity fluctuations is presumed to be determined by the mechanism responsible for their excitation, either via different emission mechanisms or mode-dependent propagation or scattering effects. The observed variations in modulation index across a mode transition would then arise from changes in the relative excitations of the two modes. Changes in  $\beta$  should be reflected by changes in the axial ratio of Q-U-V data point clusters or by changes in a mode's frequency of occurrence. If observed variations in modulation index across a mode transition are large, then the mode intensity distributions must be different to explain the observed range of  $\beta$  values. The order of the Erlang distribution for one mode would need to be  $n = 1$  to account for modulation indices as large as  $\beta = 1$ , and the order of the distribution for the other mode would need to be much greater than one to account for small values of  $\beta$ .

The assumption of Erlang mode intensities in the analysis should not be misconstrued as a claim that the intensities always follow Erlang statistics. Other probability distributions of intensity and pulse energy, such as log-normal, power law, and gamma, are possible and have been observed (e.g., Cairns et al. 2003a, 2003b; Burke-Spolaor et al. 2012). A general conclusion from the analysis, that the mean fractional linear polarization and modulation index are symmetric about a mode transition when the mode intensity distributions are identical but are asymmetric when the distributions are different, likely holds for these other distributions, as well. The log-normal distribution is of particular interest because it is frequently observed and can produce values of modulation index that are larger than those considered here.

The limit on the fractional linear polarization attributable to OPMs for low values of modulation index (Equation 46) is a familiar result. If the OPMs have the same fixed intensity, the resulting polarization and fractional polarization are both equal to zero. If the intensities then randomly vary while retaining the same mean intensity, the mean polarization and mean fractional polarization will both increase because some intensity samples will be polarized and others will not. Therefore, the mean polarization and mean fractional polarization increase as the fluctuations increase. When the intensities are identically distributed Gaussian RVs, the mean linear polarization is given by the well-known result  $L = \sigma_o \sqrt{\pi/2}$  (e.g. Papoulis 1965, p. 195), where  $\sigma_o$  is the standard deviation of the total intensity, such that the mean fractional linear polarization is  $\bar{L} = \beta \sqrt{\pi/2}$ . The constant of proportionality between  $\bar{L}$  and  $\beta$  here is different from what was derived in Equation 46, because the idealized derivation in Section 2 and MS concentrated the polarization in the Stokes parameter Q and held the Stokes parameter U fixed at zero. The limit on  $\bar{L}$  for Gaussian mode intensities



cannot increase indefinitely with increasing  $\beta$ , because the extent of the Gaussian fluctuations cannot exceed the mean to ensure the individual intensity samples are nonnegative. The upper limit on  $\beta$  for Gaussian fluctuations in this analysis is  $\beta \leq 1/(5\sqrt{2})$  (Equation 40). The limit on  $\bar{L}$  can be extended to larger values of  $\beta$  when the mode intensities are Erlang RVs, which are always nonnegative by definition, and consequently are not similarly encumbered by the limit on  $\beta$ . Erlang mode intensities extend the range of the modulation index to  $\beta \leq 1/\sqrt{2}$ , which produces a corresponding limit on the fractional linear polarization of  $\bar{L} = 1/2$ . When  $\beta$  is small ( $n \gg 1$ ), the  $\beta$  dependence of  $\bar{L}$  produced by Erlang mode intensities replicates the behavior derived from Gaussian intensities.

#### 4.2. Examples from Observations

The analysis evaluated the effectiveness of fluctuating OPM intensities in depolarizing the emission, and determined the depolarization is greatest when the mode intensities are identically distributed and the modulation index is small (Figures 5 and 6). This result suggests that mode transitions accompanied by acute depressions in linear polarization occur where the mode intensities are equal and somewhat stable, almost as if the OPMs behaved as fixed radiators. An example of this behavior occurs at the leading edge of PSR B0626+24 (Figure 2 of Weisberg et al. 1999). The pulse is almost completely linearly polarized at this location, but the polarization plunges to near-zero levels at a following mode transition. The modulation index is at its minimum value near the transition (Figure A.2 of Weltevrede et al. 2006).

The mode frequency of occurrence changes at a mode transition, and particularly so when the mode intensities are identically distributed and the modulation index is low (Figure 7). An example of this general behavior occurs in the leading component of PSR B2020+28 (Figure 3 of MS), where the linear polarization decreases abruptly at a mode transition. The PA histograms at this location (Figure 5 of MS) evolve from both modes occurring with nearly equal frequency at the transition to only one mode occurring within about six pulse phase bins. The modulation indices at this location ( $0.25 \leq \beta \leq 0.46$ ) approach the lowest value within the pulse ( $\beta = 0.18$ ; Figure 2(c) of M04). These examples suggest mode intensity fluctuations contribute to both the depolarization and the modulation of the emission.

## 5. CONCLUSIONS

A statistical model was used to explore the polarization and modulation properties of pulsar radio emission by assuming the intensities of the OPMs follow different Erlang distributions. General expressions were derived for the distributions of the resulting Stokes parameters and linear polarization. All are additive combinations of weighted Erlang distributions. General expressions for the distributions of fractional polarization and polarization position angle were also derived, and were shown to be consistent with their Gaussian counterparts when the order of the Erlang distributions is large.

A transition between the modes was examined in detail. The changing ratio of the mode mean intensities drives the transition from one mode to the other. The parameter  $m$  serves as a proxy for pulse phase and allows the behavior of the polarization and modulation statistical parameters to be resolved over the transition's duration. The fractional linear polarization and modulation index are symmetric about a transition when the mode intensity distributions are the same. The symmetry is disrupted when the distributions of mode intensities are different.

The modulation and polarization of pulsar radio emission are affected by both systematic and stochastic processes. The analysis presented in this paper focuses on a stochastic component to the emission that is affiliated with OPMs. The analysis, coupled with observational evidence, suggests the mode fluctuations contribute to the depolarization and overall modulation of the emission. If the emission is comprised solely of the stochastic component, the distributions of the mode intensities would need to be different to explain the larger variations in modulation index observed across a mode transition.

The effectiveness of superposed OPMs in depolarizing the emission was investigated. The fractional linear polarization is minimum at mode transitions where the OPM intensities are identically distributed and the modulation index of the total intensity is small. A limit on the minimum fractional linear polarization that can be attributed to the superposition of the modes as a function of modulation index was quantified. For those pulsars showing acute, deep depressions in linear polarization at a transition, the modulation index is likely small and the OPM emission is consequently quasi-stable at those locations.

### ACKNOWLEDGMENTS

The National Radio Astronomy Observatory is a facility of the National Science Foundation operated under cooperative by Associated Universities, Inc.

### REFERENCES

- Backer, D. C. & Rankin, J. M. 1980, *ApJS*, 42, 143  
 Bartel, N., Sieber, W., & Wolszczan, A. 1980, *A&A*, 90, 58  
 Burke-Spolaor, S., Johnston, S., Bailes, M., et al. 2012 *MNRAS*, 423, 1351  
 Cairns, I. H., Das, P., Robinson, P. A., & Johnston, S. 2003a, *MNRAS*, 343, 523  
 Cairns, I. H., Johnston, S., & Das, P. 2003b, *MNRAS*, 343, 512  
 Clemens, J. C. & Rosen, R. 2004, *ApJ*, 609, 340  
 Clemens, J. C. & Rosen, R. 2008, *ApJ*, 680, 664  
 Cordes, J. M. 1976a, *ApJ*, 208, 944  
 Cordes, J. M. 1976b, *ApJ*, 210, 780  
 Cordes, J. M. & Hankins, T. H. 1977, *ApJ*, 218, 484  
 Cordes, J. M., Rankin, J., & Backer, D. C. 1978, *ApJ*, 223, 961  
 Deshpande, A. A. & Rankin, J. M. 2001, *MNRAS*, 322, 438  
 Edwards, R. T. 2004, *A&A*, 426, 677  
 Edwards, R. T. & Stappers, B. W. 2004, *A&A*, 421, 681 (ES04)  
 Gil, J. A. & Sendyk, M. 2000, *ApJ*, 541, 351  
 Jenet, F. A. & Gil, J. 2003, *ApJ*, 596, L215  
 Kadri, T. & Smaili, K. 2015, *International Journal of Pure and Applied Mathematics*, 98, 81  
 Karastergiou, A., Kramer, M., Johnston, S., et al. 2002, *A&A*, 391, 247  
 Manchester, R. N., Taylor, J. H., & Huguenin, G. R. 1973, *ApJ*, 179, L7  
 Manchester, R. N., Taylor, J. H., & Huguenin, G. R. 1975, *ApJ*, 196, 83  
 McKinnon, M. M. 1997, *ApJ*, 475, 763  
 McKinnon, M. M. 2002, *ApJ*, 568, 302  
 McKinnon, M. M. 2003, *ApJ*, 590, 1026  
 McKinnon, M. M. 2004, *ApJ*, 606, 1154 (M04)  
 McKinnon, M. M. 2022, *ApJ*, 937, 92 (M22)  
 McKinnon, M. M. & Stinebring, D. R. 1998, *ApJ*, 502, 883 (MS)  
 Morris, D., Graham, D. A., & Sieber, W. 1981, *A&A*, 100, 107  
 Papoulis, A., 1965, *Probability, Random Variables, and Stochastic Processes* (New York: McGraw-Hill)  
 Rankin, J. M. 1986, *ApJ*, 301, 901  
 Rankin, J. M. & Ramachandran, R. 2003, *ApJ*, 590, 411  
 Rosen, R. & Clemens, J. C. 2008, *ApJ*, 680, 671  
 Rosen, R. & Demorest, P. 2011, *ApJ*, 728, 156  
 Ross, S. 1984, *A First Course in Probability* (New York: McMillan)  
 Ruderman, M. A. & Sutherland, P.G. 1975, *ApJ*, 196, 51  
 Smits, J. M., Stappers, B. W., Edwards, R. T. et al. 2006, *A&A*, 448, 1139  
 Stinebring, D. R., Cordes, J. M., Rankin, J. M., et al. 1984, *ApJS*, 55, 247  
 Taylor, J. H., Manchester, R. N., & Huguenin, G. R. 1975, *ApJ*, 195, 513  
 Weisberg, J. M., Armstrong, B. K., Backus, P. R., et al. 1986, *AJ*, 92, 621  
 Weisberg, J. M., Cordes, J. M., Lundgren, S. C., et al. 1999, *ApJS*, 121, 171  
 Weltevrede, P., Edwards, R. T., & Stappers, B. W. 2006, *A&A*, 445, 243  
 Weltevrede, P., Stappers, B. W., & Edwards, R. T. 2007, *A&A*, 469, 607